Desalination 531 (2022) 115694

Contents lists available at ScienceDirect

Desalination

journal homepage: www.elsevier.com/locate/desal

Energy efficiency analysis of membrane distillation for thermally regenerative salinity gradient power technologies

Doriano Brogioli [a,*], Ngai Yin Yip [b]

[a] Universität Bremen, Energiespeicher– und Energiewandlersysteme, Bibliothekstraße 1, 28359 Bremen, Germany
[b] Department of Earth and Environmental Engineering and Columbia Water Center, Columbia University, New York, NY 10027-6623, United States

HIGHLIGHTS

- Distillation coupled to salinity gradient power can convert low-grade heat to work
- Energy efficiency of membrane distillation for concentrated solutions is analyzed
- Membrane distillation has inherently lower efficiency than vacuum distillation
- Primary cause of the inefficiency is unavoidable transmembrane conductive heat loss
- Membrane distillation is worse in heat exploitation than in freshwater production

ARTICLE INFO

Keywords:
Direct contact membrane distillation
Energy efficiency
Low temperature heat sources
Renewable energy

ABSTRACT

The abundant resource of low-temperature heat sources (≈80–120 °C), e.g., low-concentration solar collectors or shallow geothermal wells, hold huge potential to be a renewable energy supply. A proposed method for harnessing such low-grade heat is to use the heat to distill a solution and then utilize the produced concentration difference to generate work, by means of salinity gradient power (SGP) technologies. In this application, the energy efficiency of the distillation process (ratio between produced mixing free energy and consumed heat) becomes a fundamental performance parameter. This study systematically analyzes the energy efficiency of direct contact membrane distillation (DCMD). This technique is often billed as an emergent membrane innovation that can use low-temperature thermal sources and additionally has the advantages of compactness and relatively simple implementation. However, we show that DCMD always has lower efficiencies than traditional vacuum distillation to achieve the same separation. In particular, the efficiency is smaller at high concentrations, which is desired for the distillation–SGP approach of energy conversion. The main source of entropy production in membrane distillation is the unavoidable thermal conduction across the membrane. Alternatively, vacuum membrane distillation could be a better candidate to regenerate the salinity gradient in low-grade heat utilization with distillation–SGP.

1. Introduction

The development of clean and renewable methods for producing mechanical work and electricity is becoming a central topic of scientific research. Some of the methods seek to exploit the vast supply of renewable heat sources by means of thermo-electric generators. Prominent examples of such heat resources include geothermal sources, industrial waste heat, and concentration solar heat collectors. Such applications are typically on large scales, but there is still a large amount of heat, available from small-scale and low-temperature (<100 °C) renewable sources, which is still not tapped due to a lack of suitable conversion technologies.

The scientific community has undertaken the challenge to develop innovative techniques to viably harvest such low-temperature thermal reservoirs, introducing radically new approaches; a literature review and analysis of the performances of some of the methods are reported in Ref. [1]. Several of the reported schemes are based on two stages and utilize an aqueous solution with a high solute concentration, as shown in Fig. 1. In the first stage, distillation, driven by the heat source, is used to separate the solution into the pure solvent and a more concentrated

* Corresponding author.
E-mail address: brogioli@uni-bremen.de (D. Brogioli).

https://doi.org/10.1016/j.desal.2022.115694
Received 27 September 2021; Received in revised form 4 March 2022; Accepted 8 March 2022
Available online 18 March 2022

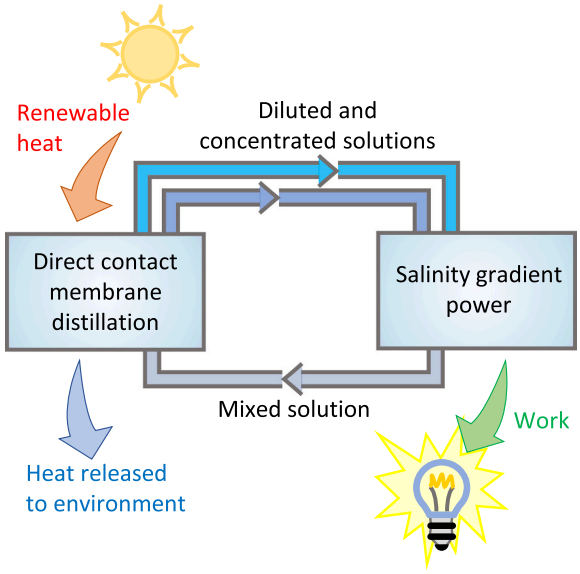

Fig. 1. Scheme of the closed loop distillation–salinity gradient power technique for producing work from a low-temperature heat source.

solution, i.e., part of the thermal energy is utilized for the Gibbs free energy of separation. The second stage is based on a "salinity gradient power" (SGP) technology, i.e., an engineered process to exploit the concentration difference between two solutions to produce useful work through. The SGP stage produces work from a portion of the mixing free energy, which is defined as the difference between the Gibbs free energy of the high and low concentration solutions and the Gibbs free energy of the solution obtained after recombining (mixing) the two. Coupling the outputs of the 1st stage distiller (the pure solvent and the concentrated solution) to the input of the 2nd stage SGP enables an overall conversion from heat to useful mechanical or electric work. In turn, the output of the SGP (diluted solution) is sent back to the distiller.

SGP has been initially developed with the aim of exploiting naturally–occurring sources of solutions with different concentration, in particular sea versus river water [2]. The original motivation for pursuing SGP, which is the reverse of desalination, is the opportunity to convert fresh water that is a locally abundant resource (and would be otherwise unutilized) to other uses, namely, energy production. In regions where water is scarce but energy is plentiful (e.g. arid countries with oil reserves) it is worth consuming energy for producing fresh water; in other regions with the reversed resource availability, it is worth doing the opposite, e.g. use river water to produce energy by means of SGP. The same reasoning applies to the use of low-temperature heat sources (low-grade heat) for desalination: the environmental conditions and the market needs will dictate if it is worth distributing the desalinated water or use it for energy generation with a distillation–SGP technology. That is, for places where the supply of water is plentiful, the low-grade heat can be converted to useful work by utilizing distillation-SGP. Conversely, for regions with water stress or scarcity, the low-grade heat should be used to distill saline feeds (by DCMD or other evaporative methods) and produce freshwater for consumption.

Various SGP technologies proposed in literature include: pressure-retarded osmosis [3], reverse electrodialysis [4,5], capacitive and battery mixing [6,7], and redox-flow batteries [8,9]. Redox-flow batteries are, by far, the most promising among the innovative techniques for the exploitation of low-temperature heat sources [1].

The application of SGP to the exploitation of low-temperature heat sources, rather than to naturally occurring solutions, is accompanied by a change of technological challenges and opportunities. On one hand, the concentrations can be much higher than in naturally occurring solutions, leading to higher power density of the SGP devices but also raising additional difficulties [1]. On the other hand, the closed loop of distillation–SGP avoids fouling, which is a main technical hurdle preventing the further advancement of sea-river water SGP [10–14].

From the thermodynamic point of view, in the above-described coupling of distillation with SGP, heat is first used to generate a mixing free energy, which is then exploited by the SGP. The net efficiency of converting thermal energy to useful work is, thus, the product of the individual efficiencies of the two stages. The efficiency of the distiller is the ratio between the Gibbs mixing free energy of the produced solutions and the consumed heat, while the efficiency of the SGP stage is the ratio between produced work and consumed Gibbs mixing free energy. The energy efficiency of several SGP technologies had been investigated in past work [11,15]. It is equally pertinent to evaluate the energy efficiency of the distillation process, i.e., the ratio between the thermal energy taken from the heat source and the produced separation work.

In traditional distillation, the feed solution is heated until it boils and the vapors are then condensed in a separate chamber. In vacuum distillation, the boiling point is depressed by removing air from the system, hence lowering the ambient pressure below the saturation vapor pressure. The heat released by the condensation of the solvent can be used for heating a second stage, operating at lower pressure (as employed in multiple-effect distillation and multi-stage flash). The energy efficiency of vacuum distillation processes has been discussed in several publications [16–19], including analyses that take into account multiple effects. These works highlighted that the 2nd-law energy efficiency of distillation can be very high, provided that extremely concentrated solutions are used, i.e., a solution with a greater elevation of the boiling point give higher efficiencies. This result could appear as counter-intuitive, especially in the field of distillation, because the boiling point elevation is often seen as an obstacle in the separation: a high boiling point elevation typically decreases the amount of produced distillate or concentrated solution per unit of heat consumed. This fact can be easily interpreted by noticing that solutions with higher boiling point elevation have more mixing free energy [16,20] (in ideal solutions, simply because they are more concentrated), thus more heat must be consumed for producing them in the separation process. This larger mixing free energy is a desired attribute in distillation–SGP thermal energy utilization, while it is unfavorable when the final aim is to produce a large amount of fresh water. Therefore, distillation–SGP approaches for the exploitation of low-temperature heat sources should, in principle, use high-concentration solutions to maximize the efficiency of the 1st separation stage.

The performances of distillation can, hence, be seen from different points of view: for the production of mixing free energy (for the coupling with an SGP technology) or the production of distillate or concentrated solution (e.g., for seawater desalination). In the case of seawater distillation, the feed solution salinity is a defined input parameter, thus the focus is on obtaining the largest amount of drinking water per unit heat energy. For this reason, it is common to characterize such techniques in terms of energy per unit volume of drinking water, termed specific energy consumption, rather than in terms of energy efficiency. In contrast, the aim of the distillation stage in heat utilization is to regenerate the salinity gradient, using the least amount of thermal energy. Hence, energy efficiency is a more useful metric.

The integration of distillation with membranes, termed direct contact membrane distillation (DCMD), has been developed. In this technique, a hydrophobic porous membrane separates the heated feed solution, from the cooled permeate of pure solvent. As the membrane material is hydrophobic, the membrane pores are not wetted by the liquids and the feed and permeate streams do not directly come into contact. Evaporation takes place from the feed and the vapors permeate across the membrane pores, eventually condensing on the permeate side. It is worth noting that the liquid-vapor phase-change in DCMD is evaporation, rather than boiling as in vacuum distillation. Some modeling and experimental work has been devoted to study the coupling of DCMD, instead of conventional distillation, with SGP technologies for

thermal energy conversion [21–25].

In this paper, we systematically analyze the energy efficiency of DCMD for generating salinity gradients. First, the model for DCMD is presented and the key mass and energy transfer equations are introduced. The profiles of temperature, permeate flux, feed solution concentration, and efficiency along the DCMD module are then examined. Next, the energy efficiency of DCMD separation at different flowrates and temperature difference of the feed and permeate streams are evaluated. The contribution of conductive heat flux to inefficiencies of the separation process is discussed. Lastly, the efficiency of DCMD is compared with vacuum distillation for different feed solution concentrations and recovery rates.

DCMD has generally lower efficiency than vacuum distillation. The study sheds light on the underlying thermodynamic principles for the lower energy efficiency of DCMD and elucidates the intrinsic performance achievable with the technology. Notwithstanding the lower efficiency, membrane distillation is attracting the interest of the scientific community because of unique advantages, in particular, the compactness and low areal footprint of the system. Our analysis shows that this technique is much less efficient than vacuum distillation under the conditions required by the distillation–SGP application, but the gap in energy–efficiency is narrowed when operating with relatively lower concentration solutions, e.g. for desalinating sea water. The results thus suggest that the research on DCMD should focus on the latter applications rather than on energy production.

2. Model of direct contact membrane distillation

2.1. Working principles of DCMD

In DCMD [26], a porous hydrophobic membrane separates the feed solution from the permeate (or distillate), as shown in Fig. 2. The hydrophobicity of the membrane material prevents the two liquids from directly coming into contact, with the air-filled pores remaining unwetted. The feed solution is heated before entering the membrane module. The solvent evaporates and the vapor permeates through the pores, reaching the colder permeate, where it condenses. In order to compare DCMD with our previous studies on vacuum distillation [16–18,20], co-current flow configuration is considered, instead of the counter-current process [22,27].

The scheme of the DCMD process is shown in Fig. 2. The process starts with two flows of liquids, pure solvent and feed solution, at temperature T_L. The steps of the process are as following:

Heating The feed solution is heated up to T_H.
Distillation The two flows enter the membrane module in co-current flow configuration. A portion of the liquid evaporates from the hot side and condenses in the cold side.
Cooling The two flows are cooled back down to T_L.

2.2. Model

The model follows Ref. [22,27]. The mass transfer is evaluated as a function of ξ, the physical position along the module, with $0 \leq \xi \leq L$ and L is the length of the module. The local temperatures of the feed solution and permeate are T_F and T_P, respectively, and are, thus, functions of ξ. It is worth noting that, at $T_F = T_P$, the vapor pressure of the permeate (pure solvent) is higher than the vapor pressure of the feed solution, thus the flux of solvent across the membrane, J, would be in the unwanted direction, towards the feed solution, i.e., mixing instead of separation. In order to reverse the flux direction and achieve the separation, corresponding to a positive J under the convention of the model presented here, the local temperature difference $T_F - T_P$ should be larger than a minimum value, called threshold temperature difference, ΔT_{th}, with ΔT_{th} defined as the temperature difference at which the vapor pressures of the feed and the permeate are equal. The local flux of solvent across the membrane, J, is assumed to be a linear function of T_F and T_P [27]:

$$J = K_m(T_F - T_P - \Delta T_{th}) \tag{1}$$

where K_m is the effective mass transfer coefficient, a characteristic property of the membrane module that can be experimentally determined.

As T_F and T_P are the temperatures of the bulk liquids and not of the solution–membrane interfaces, the experimentally measured K_m is with the effects of temperature polarization (i.e., temperature polarization is not explicitly considered in Eq. (1)). Hence, K_m describes mass transfer with the "effective" bulk temperatures that are more readily accessible in membrane characterization experiments than temperature at the solution–membrane interfaces. As a further simplifying assumption, we use a fixed value of K_m (equivalent to the mass transfer coefficient averaged across the range of operating temperatures). With a more rigorous treatment where temperature polarization is specifically considered, the flux J should vanish at a bulk temperature difference $T_F - T_P$ that is slightly larger than ΔT_{th}. However this effect is minuscule because conductive heat flux is insignificant compared to the convective heat flux. Using the effective mass transfer coefficient K_m to include the effects of temperature polarization has the advantage of being based on robust and widely adopted experimental measurements. Critically, the findings of this study, which are governed by thermodynamics, are not affected by the absolute value of K_m or temperature polarization, which are kinetic phenomena.

Eq. (1) is used in Ref. [27] to model the flux J in the presence of small temperature differences $T_F - T_P$. Since the driving force for mass transfer across the membrane is the partial vapor pressure difference, the expected dependence of J on large temperature differences should be approximately exponential. But because the effects of temperature polarization are included in the proportionality term between flux and driving force (K_m) the conversion from temperature to partial water vapor pressure (using, for example, the Antoine equation) will not be meaningful. Importantly, regardless of the use of temperature or partial vapor pressure as the driving to determine water vapor flux J, the results of the analysis are unchanged; we report in the supplementary information all the graphs of the study, but using partial pressure difference as the driving force in Eq. (1), and showed very similar qualitative behaviors.

The heat flux across the membrane has a conductive term, due to the heat conduction of the materials composing the membrane, and a convective term, due to the enthalpy of the vapor flowing through the membrane. Since enthalpy of the vapor changes across the membrane, the presence of the vapor flux affects the temperature profile and hence the conductive heat flux [27]. The conductive heat flux at the permeate-membrane interface, ζ_P, is:

$$\zeta_P = J c_{P,vap} \frac{exp\left(\frac{c_{P,vap}}{K_c} J\right)}{exp\left(\frac{c_{P,vap}}{K_c} J\right) - 1} [T_F - T_P] \tag{2}$$

where $c_{P,\,vap}$ is the specific heat of vapor and K_c is the conductive heat transfer coefficient, another characteristic property of the membrane. Analogously, the conductive heat flux at the feed-membrane interface,

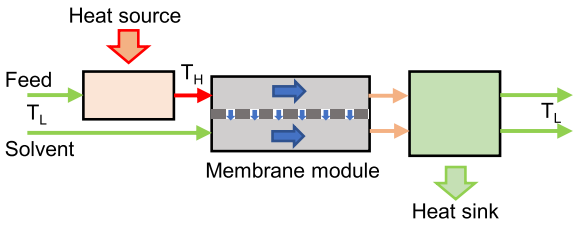

Fig. 2. Scheme of the membrane distillation process.

ζ_F, is [27]:

$$\zeta_F = Jc_{P,vap}\frac{1}{exp\left(\frac{c_{P,vap}}{K_c}J\right)-1}[T_F - T_P] \tag{3}$$

The equations above are obtained assuming that the vapor is an ideal gas. Note that ζ_P and ζ_F are not exactly identical and that the difference is related to the change of enthalpy of the vapor between the feed and the permeate sides [27]. Thus, in the limit of vanishing vapor flux, ζ_P and ζ_F become equal. After calculating ζ_P and ζ_F, the total heat flux is calculated taking into consideration the latent heat of vaporization of the solvent and the vapor flux.

We define $\Phi_F(t)$ as the molar flow of feed solution, i.e. the number of moles of solvent plus moles of solute per unit time, and $\Phi_P(t)$ as the molar flow of the permeate. Both flows are functions of axial position ξ along the membrane module. The molar flow of feed solution, Φ_F, also includes the molar flow of solute, Φ_S, which is a constant, since the solute is nonvolatile and does not pass through the membrane, i.e., it is completely rejected. The flow of permeate, Φ_P, is the total flow of solvent on the permeate side of the module, thus it also includes the initial solvent entering from the inlet.

Applying the conservation of mass:

$$\frac{\mathrm{d}}{\mathrm{d}\xi}\Phi_F = -WJ \tag{4}$$

$$\frac{\mathrm{d}}{\mathrm{d}\xi}\Phi_P = WJ \tag{5}$$

where W is the width of the membrane module. Applying the conservation of energy:

$$\frac{\mathrm{d}}{\mathrm{d}\xi}\left[H_{liq}\left(x=\frac{\Phi_S}{\Phi_F},T_F\right)\Phi_F\right] + WJH_{vap}(T_F) + W\zeta_F = 0 \tag{6}$$

$$\frac{\mathrm{d}}{\mathrm{d}\xi}\left[H_{liq}(x=0,T_P)\Phi_P\right] - WJH_{vap}(T_P) - W\zeta_P = 0 \tag{7}$$

where $H_{liq}(x,T)$ is the specific enthalpy of the solution with mole fraction x at temperature T and $H_{vap}(T)$ is the specific enthalpy of the vapor at temperature T. $H_{vap}(T)$ does not depend on pressure, since the analysis assumes that the vapor is an ideal gas. By calculating the space derivatives:

$$\frac{\partial}{\partial\Phi_F}\left[H_{liq}\left(x=\frac{\Phi_S}{\Phi_F}T_F\right)\Phi_F\right]\frac{\mathrm{d}}{\mathrm{d}\xi}\Phi_F + \frac{\partial}{\partial T_F}\left[H_{liq}\left(x=\frac{\Phi_S}{\Phi_F}T_F\right)\Phi_F\right]\frac{\mathrm{d}}{\mathrm{d}\xi}T_F + WJH_{vap}(T_F) + W\zeta_F = 0 \tag{8}$$

$$\frac{\partial}{\partial\Phi_P}\left[H_{liq}(x=0T_P)\Phi_P\right]\frac{\mathrm{d}}{\mathrm{d}\xi}\Phi_P + \frac{\partial}{\partial T_P}\left[H_{liq}(x=0T_P)\Phi_P\right]\frac{\mathrm{d}}{\mathrm{d}\xi}T_P - WJH_{vap}(T_P) - W\zeta_P = 0 \tag{9}$$

And further combining with Eq. (7):

$$-WJ\frac{\partial}{\partial\Phi_F}\left[H_{liq}\left(x=\frac{\Phi_S}{\Phi_F}T_F\right)\Phi_F\right] + \Phi_F\frac{\partial}{\partial T_F}\left[H_{liq}\left(x=\frac{\Phi_S}{\Phi_F}T_F\right)\right]\frac{d}{d\xi}T_F + WJH_{vap}(T_F) + W\zeta_F = 0 \tag{10}$$

$$WJ\frac{\partial}{\partial\Phi_P}\left[H_{liq}(x=0T_P)\Phi_P\right] + \Phi_P\frac{\partial}{\partial T_P}\left[H_{liq}(x=0T_P)\right]\frac{\mathrm{d}}{\mathrm{d}\xi}T_P - WJH_{vap}(T_P) - W\zeta_P = 0 \tag{11}$$

Accounting for the specific heat of the liquid:

$$-WJ\frac{\partial}{\partial\Phi_F}\left[H_{liq}\left(x=\frac{\Phi_S}{\Phi_F}T_F\right)\Phi_F\right] + \Phi_F c_{P,liq}\left(x=\frac{\Phi_S}{\Phi_F}T_F\right)\frac{\mathrm{d}}{\mathrm{d}\xi}T_F + WJH_{vap}(T_F) + W\zeta_F = 0 \tag{12}$$

$$WJ\frac{\partial}{\partial\Phi_P}\left[H_{liq}(x=0T_P)\Phi_P\right] + \Phi_P c_{P,liq}(x=0T_P)\frac{\mathrm{d}}{\mathrm{d}\xi}T_P - WJH_{vap}(T_P) - W\zeta_P = 0 \tag{13}$$

where $c_{P,\,liq}(x,T)$ is the specific heat of the solution with mole fraction x at temperature T. In these expressions, the derivatives with respect to Φ_F and Φ_P represent the partial molar enthalpies:

$$-WJh_{liq}\left(x=\frac{\Phi_S}{\Phi_F},T_F\right) + \Phi_F c_{P,liq}\left(x=\frac{\Phi_S}{\Phi_F},T_F\right)\frac{\mathrm{d}}{\mathrm{d}\xi}T_F + WJh_{vap}(T_F) + W\zeta_F = 0 \tag{14}$$

$$WJh_{liq}(x=0,T_P) + \Phi_P c_{P,liq}(x=0,T_P)\frac{\mathrm{d}}{\mathrm{d}\xi}T_P - WJh_{vap}(T_P) - W\zeta_P = 0 \tag{15}$$

where h_{liq} and h_{vap} are the partial molar enthalpies of the solution and of the vapor, respectively. By defining $\Lambda = h_{vap} - h_{liq}$ the vaporization enthalpy:

$$WJ\Lambda\left(x=\frac{\Phi_S}{\Phi_F},T_F\right) + \Phi_F c_{P,liq}\left(x=\frac{\Phi_S}{\Phi_F},T_F\right)\frac{\mathrm{d}}{\mathrm{d}\xi}T_F + W\zeta_F = 0 \tag{16}$$

$$-WJ\Lambda(x=0,T_P) + \Phi_P c_{P,liq}(x=0,T_P)\frac{\mathrm{d}}{\mathrm{d}\xi}T_P - W\zeta_P = 0 \tag{17}$$

These equations allow us to calculate the derivatives of the temperatures:

$$\frac{\mathrm{d}}{\mathrm{d}\xi}T_F = -W\frac{J\Lambda\left(x=\frac{\Phi_S}{\Phi_F},T_F\right)+\zeta_F}{\Phi_F c_{P,liq}\left(x=\frac{\Phi_S}{\Phi_F},T_F\right)} \tag{18}$$

$$\frac{\mathrm{d}}{\mathrm{d}\xi}T_P = W\frac{J\Lambda(x=0,T_P)+\zeta_P}{\Phi_P c_{P,liq}(x=0,T_P)} \tag{19}$$

2.3. Definitions

We define $\dot{Q}_{in}$ as the heat flow absorbed from the heat source in the heating step:

$$\dot{Q}_{in} = \left[H_{liq}\left(x=\frac{\Phi_S}{\Phi_F},T_H\right) - H_{liq}\left(x=\frac{\Phi_S}{\Phi_F},T_L\right)\right]\Phi_F \tag{20}$$

$\dot{\Delta}G$ is defined as the total flow of free energy along the membrane module:

$$\dot{\Delta}G = G_{liq}\left(x=\frac{\Phi_S}{\Phi_F(\xi=L)}T_L\right)\Phi_F(\xi=L) + \mathrm{G}_{liq}(\mathrm{x}=0\mathrm{T_L})\Phi_\mathrm{P}(\xi=\mathrm{L}) - G_{liq}\left(x=\frac{\Phi_S}{\Phi_F(\xi=0)}T_L\right)\Phi_F(\xi=0) - \mathrm{G}_{liq}(\mathrm{x}=0\mathrm{T_L})\Phi_\mathrm{P}(\xi=0) \tag{21}$$

where $G_{liq}(x,T)$ is the specific free energy of solution with mole fraction x and temperature T. The specific free energy is defined as the Gibbs free energy per mole of solution, where the moles of solution are defined as the sum of the moles of solvent and moles of solute. The terms represent

the flows of free energy through the inlets and outlets, i.e., the molar flows multiplied by the specific free energies.

The energy efficiency η is defined as:

$$\eta = \frac{\dot{\Delta} G}{\dot{Q}_{in}} \tag{22}$$

The efficiency of the Carnot cycle, η_C, is:

$$\eta_C = \frac{\Delta T}{T_H} \tag{23}$$

where $\Delta T = T_H - T_L$ is the temperature difference between heat source and heat sink. In the particular case of the process considered here, the 2nd-law efficiency, $\eta_{2nd-law}$, is the ratio between the actual efficiency and the Carnot efficiency:

$$\eta_{2nd-law} = \frac{\eta}{\eta_C} \tag{24}$$

2.4. Model input parameters

The model described above requires two empirical parameters, K_m and K_c, which describe the physical properties of the membrane. Typical values are employed for this analysis.

Following Ref. [27], we assume $K_m = 28$ mmol/(s m^2 K). This value is based on the experimental characterization of an MD membrane with a polytetrafluoroethylene active layer and a polypropylene support sublayer [28]. This K_m value and also other structural characteristics (pores of 0.2–0.4 μm, 70% porosity, total thickness of 175 μm and active layer thickness of 5–10 μm) are typical for MD membranes.

The value of K_c proposed in Ref. [27] is in the range 400–800 W/(m^2 K), calculated based on the thermal conductivity of the materials for 100 μm-thick membranes with porosity of 80%. The corresponding specific heat conductivity is in the range 0.04–0.08 W/(m K) and is consistent with values reported in literature [29,30]. We assume an intermediate value, $K_c = 600$ W/(m^2 K).

Aqueous solutions of lithium bromide are used throughout this study, because of the excellent performances of such solutions in distillation–SGP heat conversion [8,9,19]. Additionally, the electrolyte has very high solubility, which enables analysis to be performed up to high boiling point elevations. The thermodynamic parameters of the lithium bromide solutions are drawn from the data reported in Ref. [31].

3. Results and discussion

3.1. DCMD model output parameters along the module

Fig. 3a shows the temperature of the two flows along the module,

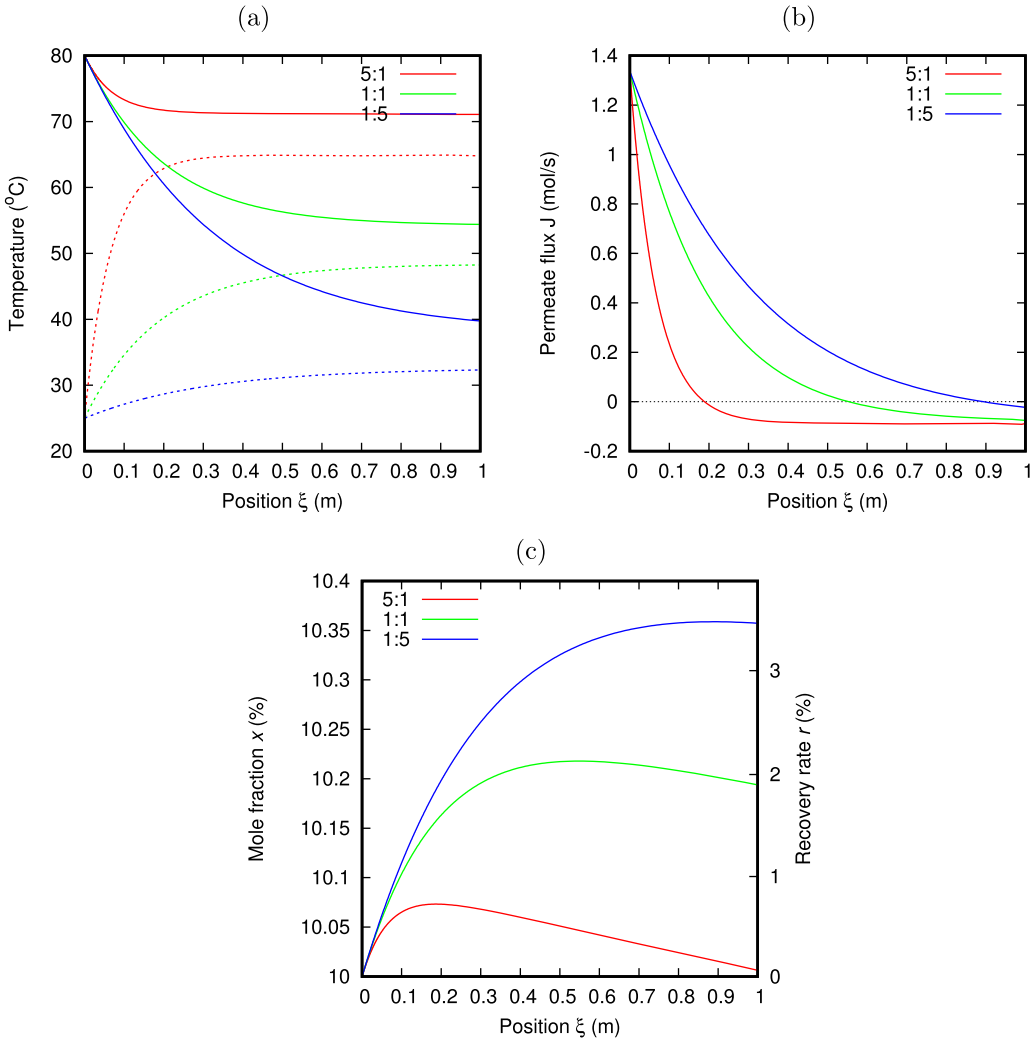

Fig. 3. Variation of physical parameters along the module: (a) temperature; (b) permeate flux; and (c) mole fraction of the feed, x, and recovery rate, r. Solution: lithium bromide, 10% mole fraction. Membrane module width: 10 cm. Initial temperatures: T_L=25 °C, T_H=80 °C. The flows Φ_F:Φ_P are 5:1, 1:1, and 1:5 mol/s. The calculation is carried out up to a length of L = 1 m.

obtained by integrating the equations along ξ. Due to evaporation from the feed solution, condensation in the permeate stream, and heat conduction from the warmer feed to cooler permeate side, the temperature difference decreases for increasing ξ. The final temperature tends to be smaller when the flow of permeate, at T_L, is large compared to the flow of feed solution.

Fig. 3b shows the permeate flux J. It decreases for increasing ξ, due to the decrease of temperature difference. It is important to notice that, due to heat conduction, the temperature difference eventually becomes smaller than ΔT_{th}. We call $L_{\max}$ the value of ξ at which this happens. For $\xi > L_{\max}$ the temperature difference is smaller than ΔT_{th}, thus the direction of vapor flux is reversed and start going from the permeate to the feed. The value of $L_{\max}$ can be seen in Fig. 3b as the value of ξ at which $J = 0$.

As the feed progresses along the module, the mole fraction increases as the solvent transport across to the permeate side (see Fig. 3c). When the permeate flux goes negative (Fig. 3b), the mole fraction experiences a turning point and starts decreasing. ΔT_{th} (threshold temperature) also increases with the higher concentration, but remains almost constant, between 7.5 and 10 K (data not shown), due to the relatively small variation of concentration along the module. Instead, $T_H - T_L = \Delta T$ decreases. At the value of ξ at which $\Delta T_{th} = \Delta T$, the vapor flux vanishes, $J = 0$. For larger ξ, the vapor flux reverses, thus the concentration decreases.

Fig. 4 shows the efficiency η of the distillation, expressed by Eq. (22). It can be noticed that the efficiency increase up to $L_{\max}$. For module lengths beyond $L_{\max}$, the permeate flux reverses its direction and the free energy of the solutions starts decreasing, leading to a decrease of efficiency. Also, the efficiency increases for increasing ratio Φ_P/Φ_F. This can be easily interpreted by noticing that the solutions at the outlet are colder for larger ratio Φ_P/Φ_F, as already shown in Fig. 3a: in turn, colder solutions at the outlet represent a lower irreversible heat exchange when they are cooled down to T_L.

As L approaches 0, the efficiency decreases effectively linearly to zero. This is because the heat consumption from the heat source is fixed (to warm the feed solution to T_H), while the amount of distilled solution is proportional to L; hence, the efficiency, which is proportional to the heat consumption normalized by amount of permeate, is essentially a straight line with respect to L.

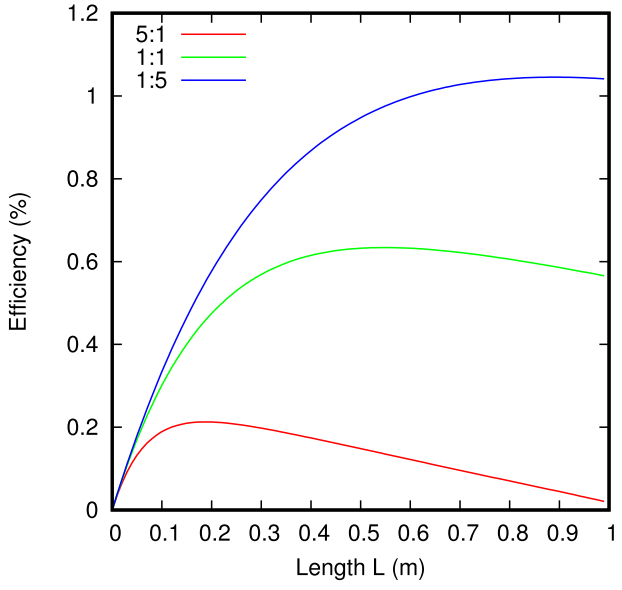

Fig. 4. Dependence of the efficiency η of distillation on the length of the module. Solution: lithium bromide, 10% mole fraction. Membrane module width: 10 cm. The flows Φ_F:Φ_P are 5:1, 1:1, and 1:5 mol/s. Initial temperatures: T_L=25 °C, T_H=80 °C.

3.2. Influence of operating parameters on efficiency

Fig. 5a shows the efficiency as a function of the ratio $\Phi_P/(\Phi_F + \Phi_P)$. For each value of the independent variable, the efficiency is evaluated at the length $L = L_{\max}$, i.e., the maximum efficiency is reported. As already noticed, the efficiency increases for increasing $\Phi_P/(\Phi_F + \Phi_P)$. In the following analysis, a ratio Φ_P:Φ_F=40:1 and a length $L = L_{\max}$ will be considered, since it represents a situation close to the maximum achievable efficiency.

The efficiency varies practically linearly as a function of $\Phi_P/(\Phi_F + \Phi_P)$ and vanishes as the ratio approaches 0. This can be seen in Fig. 5a. This fact can be understood by noticing that the recovery rate, shown in Fig. 5b, also has the same behavior of linearity with respect to the ratio $\Phi_P/(\Phi_F + \Phi_P)$. Thus, at a certain Φ_F, the amount of produced distilled water increases linearly with $\Phi_P/(\Phi_F + \Phi_P)$, while the heat consumption from the heat source remains constant, leading to the linear dependence observed for η.

Fig. 6 shows the dependence of the efficiency on the temperature difference, $\Delta T = T_H - T_L$, between the heat source and heat sink, for various initial feed concentrations. The horizontal axis intercepts represent operating DCMD with $\Delta T = \Delta T_{th}$, an initial temperature difference just equal to the threshold temperature. This operating temperature difference yields an efficiency of zero; a larger ΔT is needed to obtain positive efficiency. It can be noticed that the efficiency increases with increasing temperature difference, ΔT, for fixed mole fraction, x, until a plateau is reached (Fig. 6a). At greater mole fractions, x, the plateau efficiencies η are larger, but with the plateau occurring at higher temperature differences, ΔT. Due to this behavior, the increase in concentration at a particular temperature difference, e.g., ΔT=45 K, first gives an efficiency increase, followed by a quick decrease when the threshold temperature ΔT_{th} approaches the avaliable temperature difference, ΔT.

In order to understand these results, the efficiencies in Fig. 6a are compared with general laws. The black dotted line is Carnot's law:

$$\eta \leq \frac{\Delta T}{T_L + \Delta T} = \eta_C \tag{25}$$

The dotted lines in color represent Carati's law [16,17,20]:

$$\eta \leq \frac{\Delta T_{th}}{T_L + \Delta T_{th}} \tag{26}$$

where ΔT_{th} depends on the solute. It is important to notice that, in previous papers, the quantity ΔT_{th} was called the “boiling point elevation”, while, in the present case, the same quantity represents the threshold temperature difference. In both cases, the resulting Carati's law limiting efficiency depends on the solute properties and not on the applied temperature difference. From Fig. 6, it can be concluded that both Carnot's and Carati's laws are valid (each solid line is below the dotted line with same color). The actual efficiency is much less than the limiting values given by the above-mentioned laws.

For $\Delta T < \Delta T_{th}$, no distillation takes place and the efficiency vanishes. For ΔT slightly larger than ΔT_{th}, most of the heat is still transported by conduction rather than by evaporation and condensation. With increasing ΔT, the efficiency increases until a plateau is reached. In the range of ΔT between the onset of distillation, ΔT_{th}, and the roll-off at the beginning of the plateau, the heat conduction does not change significantly, while the heat transport by evaporation and condensation increases (due to greater vapor flux), hence the increase in efficiency. The plateau represents the range of ΔT in which the distillation is fully operating, with the maximum amount of heat transported by evaporation and condensation. Within the plateau, raising the temperature does not increase the permeate flux nor the efficiency. This is the concept behind Carati's law, which shows that the actual energy efficiency of the separation is limited by the thermophysical properties of the solutions and does not increase above a given limit, even when the applied

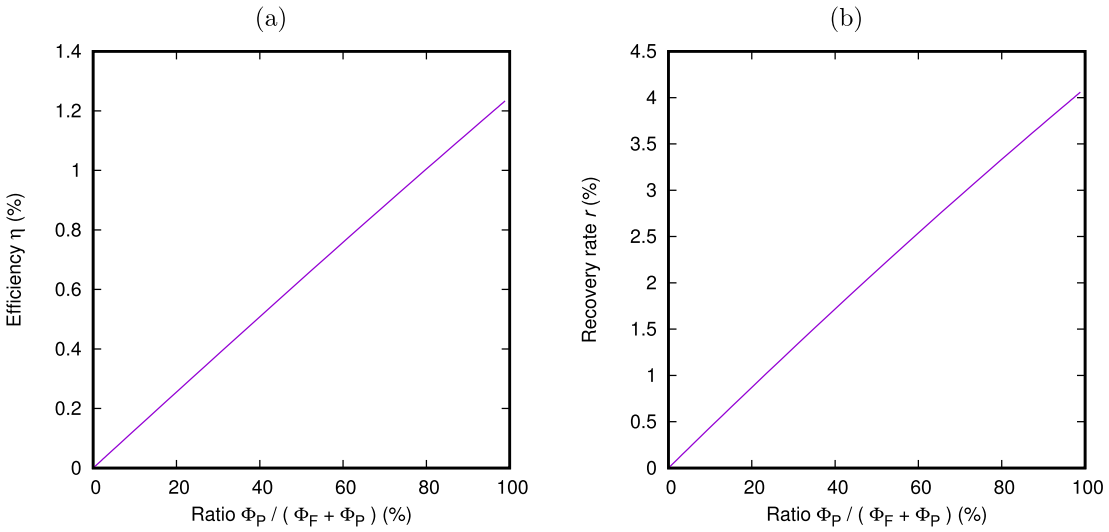

Fig. 5. Dependence of (a) the efficiency η and (b) of the recovery rate r of membrane distillation on the ratio $\Phi_P/(\Phi_F + \Phi_P)$. The length of the module is $L = L_{\max}$, which depends on the ratio. Solution: lithium bromide, 10% mole fraction. Initial temperatures: T_L=25 °C, T_H=80 °C.

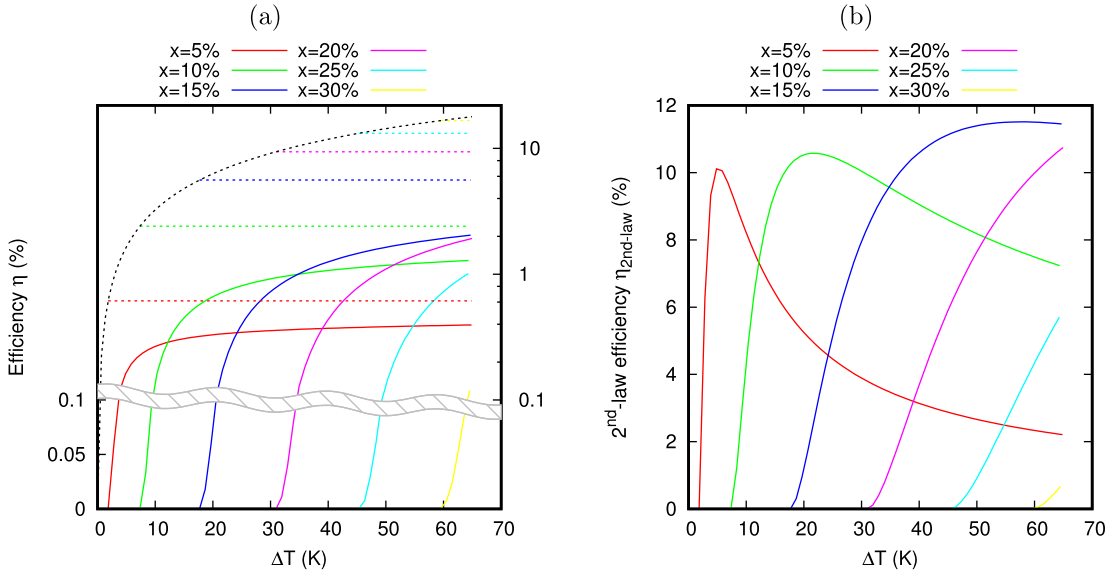

Fig. 6. Dependence of (a) the efficiency, η, and (b) second-law efficiency, $\eta_{2nd-law}$, on the temperature difference $\Delta T = T_H - T_L$ between heat source and heat sink. The ratio Φ_P/Φ_F is 40. The length of the module is $L = L_{\max}$, which depends on the ratio. Solution: lithium bromide. Initial temperatures: T_L=25 °C, $T_H = T_L + \Delta T$. Results for various values of initial mole fraction x are reported. The curves are compared with Carnot's and Carati's laws. The black dotted line represents Carnot's law. The dotted lines in color represent Carati's law for the corresponding concentration. The vertical axis of panel a has an axis break, with the scale being linear before the break (tick labels on left vertical axis) and logarithmic after the break (tick labels on right vertical axis).

temperature difference ΔT is risen. That is, Carati's law stipulates an upper bound on the achievable efficiencies for distillation that is below Carnot's limit.

In Fig. 6a, the ratio of the efficiency, η, to the Carnot efficiency, η_C, is the largest around the roll-off ΔT at the beginning of the plateau; beyond this ΔT, the ratio declines. The ratio $\eta/\eta_C = \eta_{2nd-law}$ is presented in Fig. 6b. Graphically, the maximum of the 2nd-law efficiency, $\eta_{2nd-law}$, is reached at the ΔT such that the slope of the two curves η and η_C are equal in logarithmic scale, which roughly occurs at the beginning of the plateau.

It is worth expressing Carnot's limit by defining the maximum amount of work that can be extracted from the cycle, $W_{available} = \eta_C Q_H$. Carnot's law thus states that the work, $W_{produced}$, that is actually extracted is less than $W_{available}$. The whole available work, $W_{available}$, could be ideally extracted by a thermodynamically reversible cycle. In practical cycles, actual $W_{produced}$ is less than $W_{available}$, and the work that is not extracted, $W_{available} - W_{produced}$, is proportional to the produced entropy: $\Delta S = (W_{available} - W_{produced})/T_L$. At the plateau, $W_{available}$ increases with ΔT, while $W_{produced}$ remains constant: thus, for $\Delta T \gg \Delta T_{th}$, increasing ΔT does not generate more work but, rather, only contributes to the entropy generation.

In the scenarios examined in this analysis, $W_{available} - W_{produced}$ is always a large fraction of $W_{available}$. Therefore, DCMD is far from being thermodynamically reversible and the entropy production is significant. I.e., 2nd-law efficiencies, $\eta_{2nd-law}$, for DCMD are relatively low (<15%). The ΔT at which the process operates closest to the reversibility is at the maximum of $\eta_{2nd-law}$, a value slightly larger than ΔT_{th}.

The efficiency of membrane distillation is much less than Carati's law limiting value. It is worth noting that the limit is, in principle, almost reached in vacuum distillation [16–18]. In the following, we investigate

the underlying reasons for the poor performances of membrane distillation compared with the theoretical maximum and with vacuum distillation.

3.3. Effect of heat conduction on DCMD efficiency

To investigate the influence of heat conduction in membrane distillation, we compared the energy efficiency results obtained so far with two alternative scenarios. In the first scenario, the heat conduction terms ζ_F and ζ_P are strongly decreased, by a factor 10, to represent drastically improved thermal insulation. The second scenario sets the heat conduction term to 0. Although the latter situation is purely theoretical and not physically feasible, it can provide important insights into the relevance of heat conduction. The resulting efficiencies are reported in Fig. 7. Compared with the theoretical perfectly insulating scenario (green line), the actual efficiencies with the real heat conduction values (blue line) are lower due to the additional loss of heat due to conduction. For example, at $\Delta T \approx 65$ °C, the efficiency with heat conduction is approximately half the theoretical achievable value, i.e., half of the heat is lost to undesired conduction. Inefficiencies due to heat conduction is exacerbated at lower ΔT, with the portion of energy lost being greater at smaller temperature differences. Inefficiencies can be reduced by lowering the heat conduction across the DCMD membrane. But the thermal insulation needs to be increased by several factors, rather than just incremental improvements, for the efficiency to be appreciably enhanced (red line).

In Fig. 7, the calculated efficiency is also compared with the following semi-empirical limit (dotted black line):

$$\eta \leq \frac{\Delta T_{th}}{T_L + \Delta T_{th}} \frac{\Delta T - \Delta T_{th}}{\Delta T} \tag{27}$$

It can be noticed that the limiting values expressed by Eq. (27) are relatively tight with the theoretical upper-bound scenario represented by the perfectly insulating scenario (green line). This semi-empirical limit can be justified as follows. In the right-hand side of Eq. (27), the first fraction represents the limiting value of Carati's law (Eq. (26)). The second term can be expressed as:

$$\frac{\Delta T - \Delta T_{th}}{\Delta T} = \frac{M_{vap} c_{P,liq} (\Delta T - \Delta T_{th})}{M_{vap} c_{P,liq} \Delta T} \tag{28}$$

where M_{vap} is the mass of permeated vapor. The numerator is approximately the heat transferred through evaporation and condensation along the membrane module, while the denominator is approximately the heat provided by the heat source. Thus, this term represents the intrinsic utilization of the available thermal energy for actual separation in the operation of the membrane module, which necessarily requires to provide heat for going from T_L to T_H, but then is able to exploit only the variation of enthalpy from T_H to $T_L + \Delta T_{th}$ for performing the distillation.

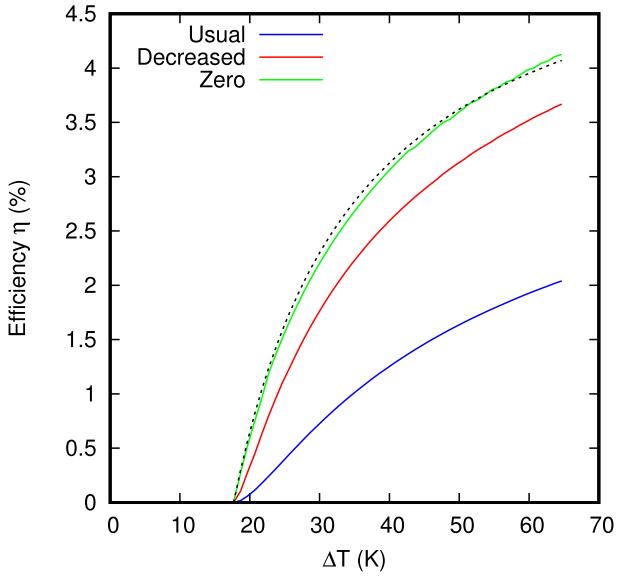

Fig. 7. Dependence of the efficiency η on the temperature difference $\Delta T = T_H - T_L$ between heat source and heat sink. The conditions are the same as for Fig. 6. The molar fraction is $x = 15\%$. Three heat conduction scenarios, represented by the heat conduction terms, ζ_F and ζ_P, were analyzed: the blue line signifies the typical heat conduction employed throughout this study; the red line denotes a more thermally insulating scenario where the heat conduction terms are decreased by a factor 10; and the green line represents perfect thermal insulation (heat conduction terms are set to zero). The dotted line is the limiting value of Eq. (27).

3.4. Comparison with vacuum distillation

It is often remarked that DCMD has advantages over traditional distillation (e.g., multi-stage flash and multiple effect distillation) by being able to work at temperatures lower than 100 °C (for aqueous solutions) and at atmospheric pressure, since the vaporization process is evaporation rather than boiling. It is however worth noting that conventional vacuum distillation also takes place at a temperature less than 100 °C, with aqueous solutions, because the pressure is suitably decreased below 1 atm to under the saturation vapor pressure of the solution. After evacuation of most of the air, the pressure is held at the desided sub-atmospheric condition by the condensation of the solvent. In industrial vacuum distillation, after the initial evacuation of air, the vacuum is maintained by a small pump with only a marginal power consumption (i.e., insignificant relative to the thermal energy input). In the closed system of the distiller and SGP device, the additional energy consumed to sustain the vacuum is expected to be almost negligible.

In this section, we report a comparison between DCMD and single-effect vacuum distillation. For both techniques, the literature discusses methods to improve the performances by recovering part of the enthalpy of condensation to heat additional volumes of solution: for DCMD, this can be done by internal heat recuperation [27], while for vacuum distillation this is commonly performed by multi-effect combination, performing a heat cascading [32]. In this section, the evaluation is done in the absence of heat recovery methods for both techniques, in order to enable a fair comparison under similar conditions. More importantly, performances with heat recovery can be approximated with reasonable accuracy from the performances in the absence of heat recovery, independent of the specific distillation technique and heat recovery method [18].

The calculation of the performances of single-effect vacuum distillation follows Ref. [16]. It takes into consideration all the significant phenomena, including the exchange of sensible heat and the variation of the boiling point which takes place due to the increase in solution concentration during the distillation.

Fig. 8 shows the comparison between the efficiencies of membrane distillation and single-effect vacuum distillation, as a function of mole fraction, at a fixed ΔT=65 K.

For the evaluation of the single-effect vacuum distillation, the pressure of the effect was selected in order to bring the average of the boiling points of the feed solution and of the solvent (i.e., pure water) in the middle of the ΔT temperature range. The efficiency of vacuum distillation is shown for two different values of the mole recovery rate r, i.e., the ratio between the moles of distilled solvent and the moles of incoming solution. It has been already observed [17] that the efficiency η has a maximum around r=25%: for this value (blue line), Fig. 8 shows that the efficiency of vacuum distillation is not too far from the Carati limit (black line). However, the recovery rate r for membrane distillation is much smaller, i.e., a much smaller amount of solvent is distilled by a single pass through the membrane (see Fig. 3c, right vertical axis). For

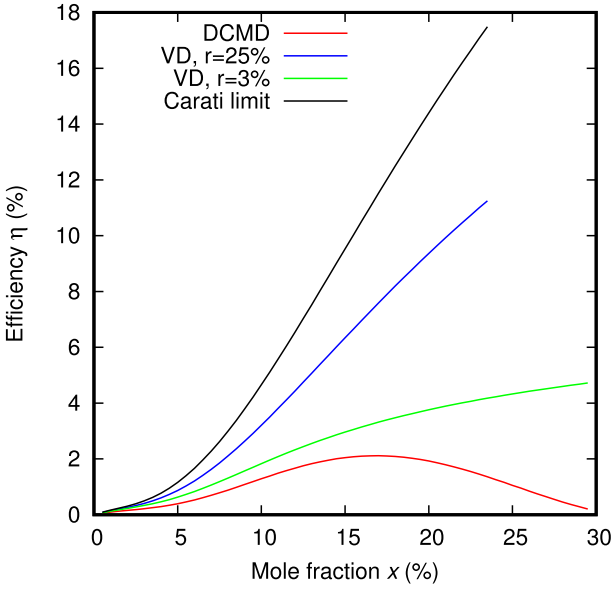

Fig. 8. Comparison between the efficiencies of membrane distillation (red line) and single-effect vacuum distillation, as a function of solution mole fraction. The parameters used for the membrane distillation are the same as for Fig. 6: the ratio Φ_P/Φ_F is 40, the length of the module is $L = L_{\max}$, and the solution is an aqueous solution of lithium bromide. The initial temperatures are T_L=25 °C and T_H=90 °C. The efficiency of vacuum distillation is reported for two values of the recovery rate r=25% and 3% (blue and green lines, respectively). The black line is the Carati limit.

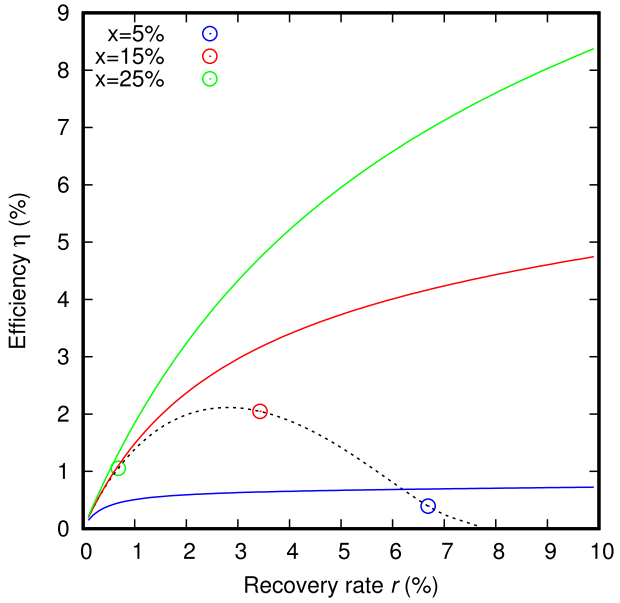

Fig. 9. Comparison between the efficiencies of membrane distillation (dotted black line) and single-effect vacuum distillation as a function of recovery rate r. Because the recovery rate of DCMD is determined by the input feed solution concentration, blue, red, and green circle symbols are indicated on the dotted black line to represent feed solutions of 5, 15, and 25% mole fraction. The blue, red, and green solid lines denote the efficiencies of the single-effect vacuum distillation, for the same concentrations of 5, 15, and 25%, respectively.

this reason, the results of single-effect vacuum distillation for r=3% is alternatively shown (green line), which is more similar to the membrane distillation performance and, hence, allows for a more equitable comparison. For this lower value of r, the efficiency of vacuum distillation is smaller. The reason is that the process requires an amount of sensible heat to bring the solution to the boiling point, which does not change regardless of the amount of produced vapor. Therefore, the less vapor is produces (r decreases), the larger is the relative contribution of the sensible heat to the total consumed heat.

In Fig. 8, we can observe that the efficiency η of the membrane distillation is even lower than the single-effect vacuum distillation for r=3% (red and green lines, respectively). A maximum is reached for DCMD at around 17% mole fraction, after which the efficiency decreases. This trend can also be observed in Fig. 6, by examining the efficiencies at ΔT=65 K for the various mole fractions. As explained in the previous section, the reason for this decrease is the increase of the heat conduction through the membrane. Overall, the performance of vacuum distillation is superior to membrane distillation and the disparity is especially pronounced at high concentration (>17% mole fraction). This is primarily because, unlike DCMD, efficiency loss due to heat conduction is practically negligible in vacuum distillation. It is worth noting that high concentrations are desired in practical cases of exploitation of low-temperature heat sources [18].

In Fig. 8 the comparison between the two technologies is done at same ΔT but different values of recovery rate r. As already discussed, this is a practically relevant comparison, since we are free to choose the recovery rate r for vacuum distillation and set it to a value that gives a large efficiency. However, for the sake of discussion of the fundamentals of the technologies, a more fair comparison can be made between the two techniques, by comparing them at same recovery rate r, so that the change in free energy of the separation ΔG is the same.

The comparison is shown in Fig. 9, for three values of feed solution mole fraction (5, 15, and 25%). For membrane distillation, the input concentration at a given temperature difference ΔT determines the recovery rate, which is represented by the dotted black line. The three points on the dotted line indicate feed solutions of 5, 15, and 25% mole fraction (blue, red, and green circle symbols, respectively). The blue, red, and green solid lines represent the efficiencies of the single-effect vacuum distillation, for the same concentrations of 5, 15, and 25%, respectively. It can be noticed that, at same recovery rate r, the vacuum distillation is always more efficient than the membrane distillation. Additionally, in vacuum distillation, the recovery rate can be adjusted to further improve the efficiency. Importantly, vacuum distillation is superior particularly at high concentrations, i.e., the desired solution property for operating the exploitation of a low-temperature heat source.

Vacuum distillation is often performed with a multi-effect configuration, i.e., by utilizing the heat in a sequence of stages (called “effects”) [32–34], in order to improve the efficiency. Analogous methods for recovering and reusing heat have also been proposed for membrane distillation [22,27]. The efficiency improvement of such techniques has been recently discussed [18], with the main finding being that the “heat recuperation” proposed for membrane systems is slightly less efficient than the multi-effect configuration used in vacuum distillation. For this reason, the comparison between the membrane module and the single-effect vacuum distillation presented in this analysis is also qualitatively valid when heat exchange and recovery is employed. Overall, vacuum distillation is still superior to membrane distillation, in particular for highly concentrated feed solutions.

4. Conclusions

This study presented a module-scale DCMD model and the energy efficiency of separation was systematically assessed. We found that the role of the threshold temperature difference, ΔT_{th}, is similar to the role played by the boiling point elevation in vacuum distillation. Separation in DCMD starts at $\Delta T > \Delta T_{th}$, with an increasing energy efficiency as ΔT increases. However, with the further increase of ΔT, the energy efficiency soon reaches a plateau and levels off. Applying a ΔT much larger than ΔT_{th} only contributes to entropy production from elevated heat transfer across an enlarged temperature difference, rather than to the

distillation.

The energy efficiency of DCMD is closer to the Carnot limit for small salt concentrations, i.e., for relatively dilute solutions, the 2nd-law efficiency is higher. This suggests that DCMD is relatively efficient in applications such as desalination of seawater; therefore, despite the lower efficiency compared with vacuum distillation, DCMD can be competitive with vacuum distillation because of the other unique advantages, in particular, the compactness and low areal footprint of the system.

On the other hand, when highly concentrated solutions are used, the threshold temperature difference, ΔT_{th}, becomes larger, imposing a corresponding increase of ΔT. In turn, this increases the thermal conduction, eventually leading to a larger entropy production and loss of efficiency. For the practical application of distillation coupled with SGP to convert low-grade heat to useful work, highly concentrated solutions that are much more saline than seawater are needed. Under these conditions, the analysis indicates that DCMD does not work efficiently and is, thus, less competitive compared with vacuum distillation, where direct heat conduction is minimal. Vacuum membrane distillation could, however, be a viable option, since it avoids the direct heat conduction, while preserving the advantages associated with membrane-based technologies, such as modular nature of the system, compactness, and the relatively straightforward implementation.

List of symbols

$c_{P,\,vap}$	Specific heat of vapor, J/(mol K)
$c_{P,\,liq}$	Specific heat of liquid, J/(mol K)
H_{liq}	Specific enthalpy of solution, J/mol
H_{vap}	Specific enthalpy of vapor, J/mol
h_{liq}	Partial molar enthalpy of solution, J/mol
h_{vap}	Partial molar enthalpy of vapor, J/mol
J	Flux of solvent across the membrane, mol/(s m^2)
K_c	Conductive heat transfer coefficient of the membrane, W/(m^2 K)
K_m	Mass transfer coefficient of the DCMD process, mol/(s K m^2)
L	Length of the membrane module, m
$L_{\max}$	Maximum useful length of the membrane module, m
N_F	Moles of feed solution, mol
N_P	Moles of permeate produced from the beginning of the process, mol
N_S	Moles of solute, mol
$\dot{Q}_{in}$	Flow of heat from the heat source, W
r	Mole recovery rate
T_F	Temperature of the feed solution, K
T_P	Temperature of the permeate, K
T_H	Temperature of the heat source, K
T_L	Temperature of the heat sink, K
W	Width of the membrane module, m
$W_{produced}$	Work produced by the process, J
$W_{available}$	Maximum work that can be produced, J
x	Mole fraction of the feed solution
ζ_F	Conductive heat flux at the feed-membrane interface, W/m^2
ζ_P	Conductive heat flux at the permeate-membrane interface, W/m^2
ΔT	Temperature difference $T_H - T_L$, K
ΔT_{th}	Threshold temperature difference, K
$\dot{\Delta} G$	Flow of mixing free energy, W
η	Energy efficiency,
η_C	Efficiency of the Carnot cycle
$\eta_{2nd-law}$	2nd law efficiency
Λ	Latent heat of vaporization, J/mol
Φ_F	Molar flow in the feed side of the membrane, mol/s
Φ_P	Molar flow in the permeate side of the membrane, mol/s
Φ_S	Molar flow of solute in the feed side of the membrane, mol/s
ξ	Axial position along the membrane module, m

CRediT authorship contribution statement

Doriano Brogioli: Conceptualization; Methodology; Formal analysis; Data curation; Visualization; Validation; Investigation; Writing - original draft; Writing - review & editing.
Ngai Yin Yip: Conceptualization; Methodology; Validation; Investigation; Writing - original draft; Writing - review & editing.

Declaration of competing interest

The authors declare that they have no known competing financial interests or personal relationships that could have appeared to influence the work reported in this paper.

Appendix A. Supplementary data

Supplementary data to this article can be found online at https://doi.org/10.1016/j.desal.2022.115694.

References

[1] D. Brogioli, F. La Mantia, Innovative technologies for energy production from low temperature heat sources: critical literature review and thermodynamic analysis, Energy Environ. Sci. 14 (2021) 1057–1082.
[2] J.D. Isaacs, R.J. Seymour, The ocean as a power resource, Int. J. Environ. Stud. 4 (1973) 201–205.
[3] A. Altaee, P. Palenzuela, G. Zaragoza, A.A. AlAnezi, Single and dual stage closed-loop pressure retarded osmosis for power generation: feasibility and performance, Appl. Energy 191 (2017) 328–345.
[4] A. Tamburini, M. Tedesco, A. Cipollina, G. Micale, M. Ciofalo, M. Papapetrou, W. Van Baak, A. Piacentino, Reverse electrodialysis heat engine for sustainable power production, Appl. Energy 206 (2017) 1334–1353.
[5] B. Ortega-Delgado, F. Giacalone, A. Cipollina, M. Papapetrou, G. Kosmadakis, A. Tamburini, G. Micale, Boosting the performance of a reverse electrodialysis - multi-effect distillation heat engine by novel solutions and operating conditions, Appl. Energy 253 (2019), 113489.
[6] M. Marino, L. Misuri, A. Carati, D. Brogioli, Proof-of-concept of a zinc-silver battery for the extraction of energy from a concentration difference, Energies 7 (6) (2014) 3664–3683.
[7] M. Marino, L. Misuri, A. Carati, D. Brogioli, Boosting the voltage of a salinity-gradient-power electrochemical cell by means of complex-forming solutions, Appl. Phys. Lett. 105 (2014), 033901.
[8] I. Facchinetti, R. Ruffo, F. La Mantia, D. Brogioli, Thermally-regenerable redox flow battery for exploiting low-temperature heat sources, Cell Rep. Phys. Sci. 1 (5) (2020), 100056.
[9] I. Facchinetti, E. Cobani, D. Brogioli, F. La Mantia, R. Ruffo, Thermally regenerable redox flow battery, ChemSusChem 13 (2020) 5460–5467.
[10] N.Y. Yip, M. Elimelech, Influence of natural organic matter fouling and osmotic backwash on pressure retarded osmosis energy production from natural salinity gradients, Environ. Sci. Technol. 47 (21) (2013) 12607–12616.
[11] N.Y. Yip, D. Brogioli, H. Hamelers, K. Nijmeijer, Salinity gradients for sustainable energy: primer, progress, and prospects, Environ. Sci. Technol. 50 (22) (2016) 12072–12094.
[12] W.R. Thelin, E. Sivertsen, T. Holt, G. Brekke, Natural organic matter fouling in pressure retarded osmosis, J. Membr. Sci. 438 (2013) 46–56.
[13] D.A. Vermaas, D. Kunteng, M. Saakes, K. Nijmeijer, Fouling in reverse electrodialysis under natural conditions, Water Res. 47 (3) (2013) 1289–1298.
[14] M. Mossad, L. Zou, Study of fouling and scaling in capacitive deionisation by using dissolved organic and inorganic salts, J. Hazardous Materials 244–245 (2013) 387–393.
[15] N.Y. Yip, M. Elimelech, Thermodynamic and energy efficiency analysis of power generation from natural salinity gradients by pressure retarded osmosis, Environ. Sci. Technol. 46 (9) (2012) 5230–5239.
[16] D. Brogioli, F. La Mantia, N.Y. Yip, Thermodynamic analysis and energy efficiency of thermal desalination processes, Desalination 428 (2018) 29–39.
[17] D. Brogioli, F. La Mantia, N.Y. Yip, Energy efficiency analysis of distillation for thermally regenerative salinity gradient power technologies, Renew. Energy 133 (2019) 1034–1045.
[18] D. Brogioli, F. La Mantia, Heat recovery in energy production from low temperature heat sources, AIChE J. 65 (2019) 980–991.
[19] F. Giacalone, C. Olkis, G. Santori, A. Cipollina, S. Brandani, G. Micale, Novel solutions for closed-loop reverse electrodialysis: thermodynamic characterisation and perspective analysis, Energy 166 (2019) 674–689.
[20] A. Carati, M. Marino, D. Brogioli, Thermodynamic study of a distiller-electrochemical cell system for energy production from low temperature heat sources, Energy 93 (1) (2015) 984–993.

[21] K.L. Hickenbottom, J. Vanneste, L. Miller-Robbie, A. Deshmukh, M. Elimelech, M. B. Heeley, T.Y. Cath, Techno-economic assessment of a closed-loop osmotic heat engine, J. Membr. Sci. 535 (2017) 178–187.
[22] S.H. Lin, N.Y. Yip, T.Y. Cath, C.O. Osuji, M. Elimelech, Hybrid pressure retarded osmosis-membrane distillation system for power generation from low-grade heat: thermodynamic analysis and energy efficiency, Environ. Sci. Technol. 48 (9) (2014) 5306–5313.
[23] E. Shaulsky, C. Boo, S.H. Lin, M. Elimelech, Membrane-based osmotic heat engine with organic solvent for enhanced power generation from low-grade heat, Environ. Sci. Technol. 49 (9) (2015) 5820–5827.
[24] R. Long, B. Li, Z. Liu, W. Liu, Hybrid membrane distillation-reverse electrodialysis electricity generation system to harvest low-grade thermal energy, J. Membr. Sci. 525 (2017) 107–115.
[25] M. Micari, A. Cipollina, F. Giacalone, G. Kosmadakis, M. Papapetrou, G. Zaragoza, G. Micale, A. Tamburini, Towards the first proof of the concept of a reverse electrodialysis - membrane distillation heat engine, Desalination 453 (2019) 77–88.
[26] A.M. Alklaibi, N. Lior, Membrane-distillation desalination: status and potential, Desalination 171 (2005) 111–131.
[27] S. Lin, N.Y. Yip, M. Elimelech, Direct contact membrane distillation with heat recovery: thermodynamic insights from module scale modeling, J. Membr. Sci. 453 (2014) 498–515.
[28] T.Y. Cath, V.D. Adams, A.E. Childress, Experimental study of desalination using direct contact membrane distillation: a new approach to flux enhancement, J. Membr. Sci. 228 (1) (2004) 5–16.
[29] K.W. Lawson, D.R. Lloyd, Membrane distillation. II. Direct contact MD, J. Membr. Sci. 120 (1) (1996) 123–133.
[30] R.W. Schofield, A.G. Fane, C.J.D. Fell, Heat and mass-transfer in membrane distillation, J. Membr. Sci. 33 (3) (1987) 299–313.
[31] Z. Yuan, K.E. Herold, Thermodynamic properties of aqueous lithium bromide using a multiproperty free energy correlation, HVAC&R Res. 11 (3) (2005) 377–393.
[32] K. Mistry, M.A. Antar, J.H. Lienhard V, An improved model for multiple effect distillation, Desalination and Water Treatment 51 (2013) 807–821.
[33] A.D. Khawaji, I.K. Kutubkhanah, J.M. Wie, Advances in seawater desalination technologies, Desalination 221 (1–3) (2008) 47–69.
[34] S.A. Kalogirou, Seawater desalination using renewable energy sources, Prog. Energy Combust. Sci. 31 (3) (2005) 242–281.